Odontology
https://doi.org/10.1007/s10266-026-01475-4

ORIGINAL ARTICLE

Influence of printing orientation on the mechanical and surface characteristics of a novel 3D-printed definitive resin-based composite

Nazire Esra Ozer[1] · **Zeynep Sahin**[1] · **Mehmet Ali Kilicarslan**[2]

Received: 22 March 2026 / Accepted: 14 June 2026
© The Author(s) 2026

Abstract

This study evaluated the effects of different printing orientations on the mechanical properties and surface roughness of a 3D-printed definitive resin-based composite (RBC) material. Bar shaped samples were fabricated from a 3D-printed RBC (VarseoSmile TriniQ) using three different build orientations (0°, 45°, and 90°) and lithium disilicate ceramic (IPS e.max CAD). Flexural strength and elastic modulus were evaluated using a three point bending test. Surface microhardness was assessed with a Vickers hardness test, and surface roughness was measured using a contact profilometer. Following mechanical testing, the sample surfaces and fractured regions were further examined by scanning electron microscopy (SEM) for topographic and fractographic evaluation. Statistical analysis was performed at $\alpha = 0.05$ using one way ANOVA, with post hoc comparisons conducted using the Tamhane test. Significant differences were observed among the tested materials for all evaluated parameters ($p < 0.001$). IPS group demonstrated superior mechanical properties and lower surface roughness compared to the 3D-printed RBCs. Within the 3D-printed groups, the 0° build orientation exhibited higher flexural strength, whereas the 90° orientation showed increased surface hardness. Elastic modulus and surface roughness were not significantly influenced by printing orientation ($p > 0.05$). SEM analyses supported the quantitative findings by revealing a homogeneous and compact microstructure in IPS group and orientation-dependent surface and fracture features in the 3D-printed RBC groups. IPS e.max CAD demonstrated superior mechanical performance. The 0° orientation improved flexural strength, while the 90° orientation enhanced surface hardness, suggesting that build orientation should be selected according to the intended clinical function.

Keywords 3D printing · Resin-based composites · Build orientation · Flexural strength · Elastic modulus · Surface roughness · Surface hardness

Introduction

In recent years, advances in filler technology, bonding systems, and polymer chemistry have substantially expanded the range of restorative materials available in dentistry [1]. In this context, three-dimensional (3D) -printed resin-based composites (RBCs) developed for permanent restorations have emerged as a viable alternative to conventionally milled computer-aided design and computer-aided manufacturing (CAD/CAM) composite materials [2]. Owing to their compatibility with digital workflows, increased design flexibility, and the potential for more efficient fabrication processes, these materials have attracted growing interest in both clinical applications and experimental research settings [1, 3].

Advances in materials science have enabled the incorporation of ceramic-based fillers into resin matrices, allowing 3D-printed RBCs to reach a level of mechanical, biological, and physical performance suitable for use as permanent restorative materials [4]. Concurrently, the type, content, particle size, morphology, and spatial distribution of these fillers within the matrix play a critical role in defining surface characteristics, mechanical behavior, and dimensional accuracy [3]. Although ceramic fillers are primarily introduced to enhance mechanical strength, their presence may

✉ Zeynep Sahin
zeynep.sahin@lokmanhekim.edu.tr

[1] Department of Prosthodontics, Faculty of Dentistry, Lokman Hekim University, Söğütözü. 2179 St, Çankaya, Ankara 06510, Turkey

[2] Department of Prosthodontics, Faculty of Dentistry, Ankara University, Yenimahalle, Ankara, Turkey

Published online: 30 June 2026

increase material viscosity, which can adversely affect the flow behavior, printing accuracy, and layer formation during the additive manufacturing process [5, 6]. In addition, increased light scattering and refractive index mismatch associated with filler particles may reduce the polymerization depth [7] and weaken interlayer bonding, ultimately compromising mechanical integrity and dimensional stability [5, 6].

For these reasons, many 3D-printed RBCs have initially been developed for single unit restorations and therefore show limitations when applied to broader clinical indications that involve more complex geometries and higher mechanical demands [2]. To address these limitations, a newly developed resin material, VarseoSmile TriniQ (BEGO, Bremen, Germany), has been introduced for use not only in single crowns but also in 3-unit fixed dental prostheses (FDPs) [8–11]. TriniQ is described as a hybrid resin based composite consisting of a methacrylate based organic matrix, with approximately 55–80 wt% organic monomers and 20–45 wt% ceramic based inorganic fillers. According to the manufacturer provided technical data, this filler composition is intended to balance mechanical strength and dimensional stability while maintaining a viscosity and printing accuracy suitable for digital light processing (DLP) -based 3D printing workflows [12].

The performance of 3D-printed RBCs is influenced by multiple factors beyond resin composition alone [13, 14], including the 3D printing system employed [5, 15, 16], processing parameters [11, 13, 17], and post-curing protocols [7, 18]. Among these variables, printing orientation remains a subject of ongoing debate, as it may intensify the stair-step effect and contribute to interlayer surface irregularities [8, 11, 13]. Such effects can compromise surface integrity, reduce manufacturing efficiency, and adversely affect dimensional accuracy [19]. Accordingly, careful consideration of these process-related factors is essential for achieving restorations with reliable and predictable mechanical performance [2, 20].

Although 3D-printed RBCs have demonstrated increasing potential in prosthetic dentistry, their clinical applications remain at an early stage [21]. Current evidence regarding their long-term durability, optimal clinical indications, and performance under intraoral conditions is limited [2]. In particular, studies focusing on definitive 3-unit FDPs fabricated using 3D printing are quite limited [1, 5, 8, 10, 11, 13, 22–24]. Moreover, the existing literature includes only a limited number of investigations that simultaneously address both the mechanical properties [5, 13] and surface characteristics [1, 3] of these restorations. Therefore, a comprehensive evaluation of the mechanical and surface-related behavior of these emerging materials is essential to better define their potential clinical indications prior to broader clinical adoption.

In this context, the present study aimed to investigate the effect of different printing orientations on the mechanical properties, including flexural strength, elastic modulus, and microhardness, as well as on the surface roughness of a newly developed reinforced resin material designed for permanent 3-unit FDPs, namely, VarseoSmile TriniQ. In addition, scanning electron microscopy (SEM) was used to provide a detailed assessment of surface topography and to perform fractographic analysis of the fracture surfaces following mechanical testing. To identify the most appropriate printing conditions, specimens fabricated from 3D-printed RBCs were compared with those produced from lithium disilicate based IPS e.max CAD, a reference material widely used in clinical practice for a broad range of indications, including 3-unit FDPs supported distally by a second premolar, due to its high mechanical strength, reliable fit, and satisfactory esthetic performance. The null hypotheses of this study were as follows: (i) printing orientation has no statistically significant effect on mechanical properties (flexural strength, elastic modulus, and microhardness); (ii) printing orientation does not significantly influence surface roughness.

Materials and methods

The sample size was determined using G*Power software (version 3.1.9.2; Heinrich Heine University Düsseldorf, Düsseldorf, Germany). Based on an assumed effect size of 0.50, a statistical power of 90%, and a significance level of $\alpha = 0.05$, a minimum of 12 specimens per group was required, resulting in a total sample size of 48 specimens. In addition, one representative specimen from each subgroup was selected for qualitative surface topography and fractographic evaluation using scanning electron microscopy (SEM). The materials evaluated in the present study and their compositions are summarized in Table 1, and the overall experimental design is schematically illustrated in Fig. 1.

Preparation of test samples

Two material groups were included in this study: a 3D-printed RBC, VarseoSmile TriniQ (BEGO, Bremen, Germany), and lithium disilicate glass-ceramic, IPS e.max CAD (Ivoclar Vivadent, Schaan, Liechtenstein). The bar-shaped samples were prepared in accordance with ISO 6872:2015, which defines standardized dimensions and testing requirements for the mechanical characterization of dental restorative materials [25]. Accordingly, the sample dimensions were set at 25 × 4 × 3 mm (length × width × thickness) [26].

Table 1 Overview of test groups

Group names	Materials	Chemical composition	Manufacturing method	Manufacturer
IPS	IPS e.max CAD	SiO_2: 57–80%, Li_2O: 11–19%, K_2O: 0–13%, P_2O_5: 0–11%, ZrO_2: 0–8%, ZnO: %0–8% Coloring oxides: 0–8%	Sliced with diamond saw	Ivoclar Vivadent, Schaan, Lihtenştayn
RBC-0	VarseoSmile Triniq	Organic matrix: Esterification products of 4,4′-isopropylidenediphenol, ethoxylated, and 2-methylprop-2-enoic acid: 55–80 wt%, benzeneacetic acid,	3D printing with 90-degree build orientation	Bego, Bremen, Germany
RBC-45		alpha-oxo-, methyl ester < 5 wt%, diphenyl (2,4,6-trimethylbenzoyl) phosphine oxide < 2.5 wt%, titanium dioxide:	3D printing with 45-degree build orientation	
RBC-90		< 2.5 wt Inorganic fillers: ceramic fillers	3D printing with 0-degree build orientation	

SiO_2 Silicon dioxide, *Li_2O* Lithium oxide, *K_2O* Potassium oxide, *P_2O_5* Phosphorus pentoxide, *ZrO_2* Zirconium dioxide, *ZnO* Zinc oxide

The bar samples were digitally designed using dental CAD software (Exocad DentalCAD; Exocad GmbH, Darmstadt, Germany) and exported in the standard tessellation language (STL) format. TriniQ specimens were fabricated using a digital light processing (DLP)-based 3D printer (BEGO Varseo XS; BEGO, Bremen, Germany) with three different build orientations (0°, 45°, and 90°). Support structures were automatically generated by the printing software, and the layer thickness was fixed at 50 µm. Post-processing procedures were performed in strict accordance with the manufacturer's recommendations [9]. Following printing, the specimens were ultrasonically cleaned in 96% ethanol for 5 min and air-dried at room temperature. Subsequently, post-curing was performed using a dedicated curing unit (Otoflash G171; NK Optik, Baierbrunn, Germany) under a nitrogen atmosphere. The post-curing protocol consisted of two cycles of 1500 flashes, delivered at a wavelength range of 360–410 nm with an irradiance of 12.5 mW/cm² per flash.

Test samples fabricated from IPS e.max CAD blocks were sectioned to the target dimensions (25 × 4 × 3 mm) using a diamond precision saw under water cooling (Micracut 201; Metkon, Bursa, Türkiye). To achieve the final mechanical properties and ensure full crystallization of the lithium disilicate ceramic, a crystallization process was subsequently performed in accordance with the manufacturer's recommendations [27]. This procedure was carried out using a ceramic furnace (Programat P510; Ivoclar Vivadent, Schaan, Liechtenstein). The crystallization cycle was initiated at 403 °C with a holding time of 6 min, followed by heating at a rate of 90 °C/min to 820 °C, where the temperature was maintained for 7 min. Vacuum was applied between 550 and 820 °C, and the program was completed at a final temperature of 700 °C.

After fabrication, all samples were sequentially polished using 600-, 800-, and 1200-grit silicon carbide (SiC) abrasive papers (Buehler GmbH, Düsseldorf, Germany) to ensure dimensional standardization. The sample dimensions were verified using a digital caliper (Mitutoyo Corp., Tokyo, Japan) with an accuracy of ± 0.01 mm to ensure compliance with ISO specifications.

Artificial aging was performed by thermocycling the samples between 5 and 55 °C for 5000 cycles, with a dwell time of 30 s at each temperature, using a thermocycling device (SD Mechatronic Thermocycler; Julabo GmbH, FT 200, Seelbach, Germany). After thermocycling, all samples were ultrasonically cleaned in distilled water for 10 min (Steris Reliance Sonic 250; Soma Tech Intl., USA) to remove surface residues prior to further testing.

Three-point bending test

The flexural properties of the samples were evaluated using a three-point bending test performed on a universal testing machine (Lloyd LRX; Lloyd Instruments, Fareham, Hampshire, UK). The test was conducted in accordance with ISO 6872, with a support span of 20 mm. All samples were loaded at a crosshead speed of 1 mm/min until fracture, and the maximum load at failure was recorded in Newtons (N).

Flexural strength (σ) was calculated using the following equation:

$$\sigma = 3Fl/2wh^2$$

In addition, the elastic modulus (E) was determined from the linear portion of the load-deflection curve using the following equation:

$$E = Fl^3/4wh^3d$$

In these equations, F represents the maximum load at the fracture (N), l the support span (20 mm), w the specimen width (4 mm), h the specimen thickness (3 mm), and d the deflection corresponding to load F.

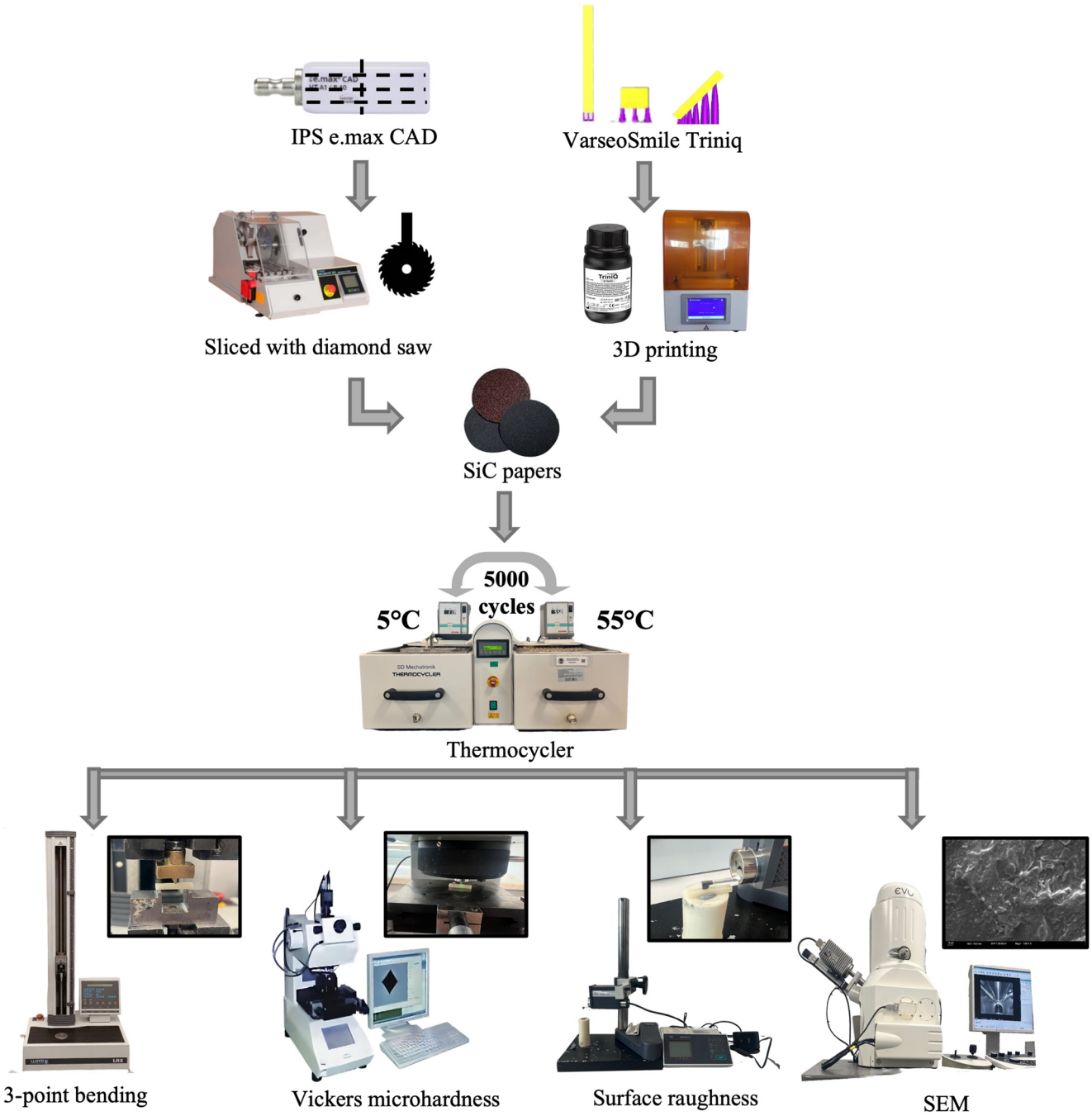


Fig. 1 Schematic illustration of the experimental workflow

Microhardness analysis

The surface microhardness of the bar-shaped samples was determined using a Vickers microhardness tester (Shimadzu HMV; Shimadzu Corp., Tokyo, Japan). A load of 200 g was applied to each sample for a dwell time of 10 s. For each sample, three indentations were made at randomly selected locations on the surface, ensuring adequate spacing between indentations to avoid interaction effects.

The Vickers hardness value (HV) was calculated using the following equation:

$$HV = 1.854 \times \left(F/d^2\right)$$

where F is the applied load (kgf), and d is the mean diagonal length of the indentation (mm).

After indentation, the dimensions of each imprint were automatically measured using the integrated image analysis

software (Mares ImPA_hrd_061.vi). The hardness values were recorded as Vickers Hardness Numbers (VHN). For each sample, the mean of the three measurements was calculated and used as the representative microhardness value for statistical analysis.

Surface roughness analysis

The surface roughness of the samples was evaluated using a contact profilometer (Perthometer; Mahr GmbH, Ingolstadt, Germany). Measurements were performed with a tracing length of 5.5 mm and a cut off value of 0.8 mm. For each sample, the surface roughness was recorded at three randomly selected locations along the surface, and the arithmetic mean of these measurements was calculated. The average surface roughness values (Ra, µm) were included in the statistical analysis.

Scanning electron microscopy (SEM) analysis

Scanning electron microscopy (SEM) was employed to characterize the surface morphology and fracture behavior of the samples subjected to the three point bending test. Within the scope of the analysis, the intact upper surfaces of the samples were examined to assess the surface topography, whereas the fractured sections generated after mechanical testing were evaluated from a fractographic perspective. Prior to SEM observation, the non conductive samples were coated with a thin layer of gold using a rotary vacuum sputter coater to ensure electrical conductivity. Microstructural examinations were performed using a tabletop SEM system (EVO 40; Carl Zeiss AG, Oberkochen, Germany). The imaging parameters were adjusted according to the type of analysis performed. Surface topography including layer formation, surface irregularities, and micro defects was examined at magnifications ranging from 500× to 5000×. Fractographic analysis focused on the evaluation of fracture surface morphology, including surface roughness characteristics, crack path features, lamellar structures, micro-voids, and fragmented regions, which were primarily examined at magnifications ranging from 60× to 1000×.

Statistical analysis

The statistical analysis of the data was performed using SPSS (version 29.0.1.0; IBM Corp., Armonk, NY, USA). Normality of distribution was determined using the Shapiro–Wilk and Kolmogorov–Smirnov tests. To determine the differences between more than two independent groups, a one-way analysis of variance (ANOVA) test was used. Homogeneity of variances was assessed using the Levene test. To determine the difference between two independent groups, the post hoc Tamhane test was used. Statistical data are expressed as the mean and standard deviation. The significance level was set at 0.05.

Result

The mean values and standard deviations obtained from the flexural strength, elastic modulus, microhardness, and surface roughness tests of the material groups are presented in Table 2. According to the one-way ANOVA results, statistically highly significant differences were detected among the groups for all evaluated parameters ($p<0.001$).

The IPS group exhibited the highest mechanical performance among all the tested groups, with a flexural strength of 281.22 MPa and an elastic modulus of 77.20 GPa ($p<0.001$). When the 3D-printed RBC groups were analyzed separately, specimens fabricated with a 0° build orientation (85.96 MPa) showed significantly higher flexural strength than those printed at 90° (65.41 MPa) and 45° (56.02 MPa). In contrast, no statistically significant difference was observed among the build orientations of the 3D-printed RBC groups in terms of elastic modulus ($p>0.05$).

Evaluation of the microhardness data showed that the IPS group (259.61 VHN) exhibited the highest surface hardness among all tested materials, followed by the RBC-90, RBC-0, and RBC-45 groups, with statistically significant differences observed between the groups ($p<0.001$). Within the 3D-printed groups, the 90 degree build orientation (32.83 VHN) was associated with increased surface hardness.

Table 2 Flexural strength, elastic modulus, microhardness, and surface roughness values of the test groups

Test Groups	Flexural Strength (MPa)	Elastic modulus (GPa)	Microhardness (VHN)	Surface roughness (µm)
IPS	281.22 ± 39.38^{a}	77.20 ± 6.48^{a}	259.61 ± 12.07^{a}	0.10 ± 0.02^{a}
RBC-0	85.96 ± 14.16^{b}	5.65 ± 0.60^{b}	20.76 ± 2.92^{b}	0.37 ± 0.04^{b}
RBC-45	56.02 ± 7.15^{c}	5.23 ± 0.28^{b}	17.16 ± 2.97^{c}	0.34 ± 0.04^{b}
RBC-90	65.41 ± 6.65^{d}	5.31 ± 0.38^{b}	32.83 ± 5.43^{d}	0.39 ± 0.06^{b}
P value	**<0.001**	**<0.001**	**<0.001**	**<0.001**

IPS IPS e.max CAD; *RBC* VarseoSmile TriniQ 3D-printed restorations − 90°, 45°, and 0° build orientations

Data are presented as mean ± SD. Statistically significant p values are bolded (*$p<0.05$)

Different superscripts in the vertical columns indicate statistically significant differences between groups

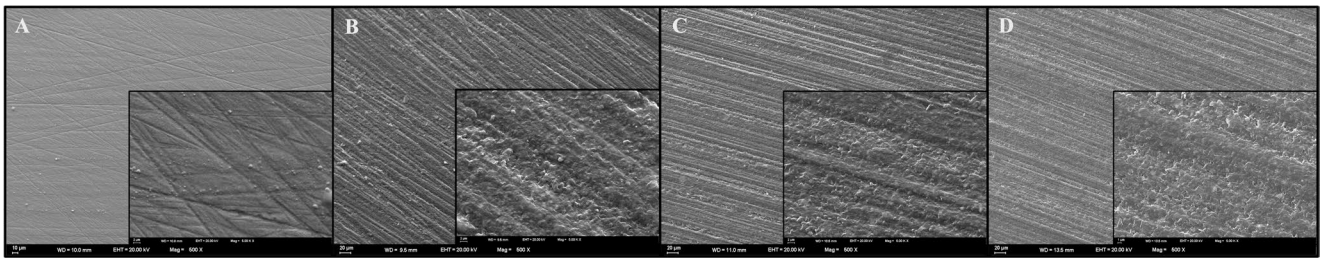


Fig. 2 Representative SEM images of the flat surface topography of the tested groups. (**A**) IPS: IPS e.max CAD, (**B**) RBC-0: VarseoSmile TriniQ 3D printed at 0° orientation, (**C**) RBC-45: VarseoSmile TriniQ 3D printed at 45° orientation, (**D**) RBC-90: VarseoSmile TriniQ 3D printed at 90° orientation. Low-magnification images were obtained at 500×, and the corresponding higher-magnification insets were recorded at 5.000×

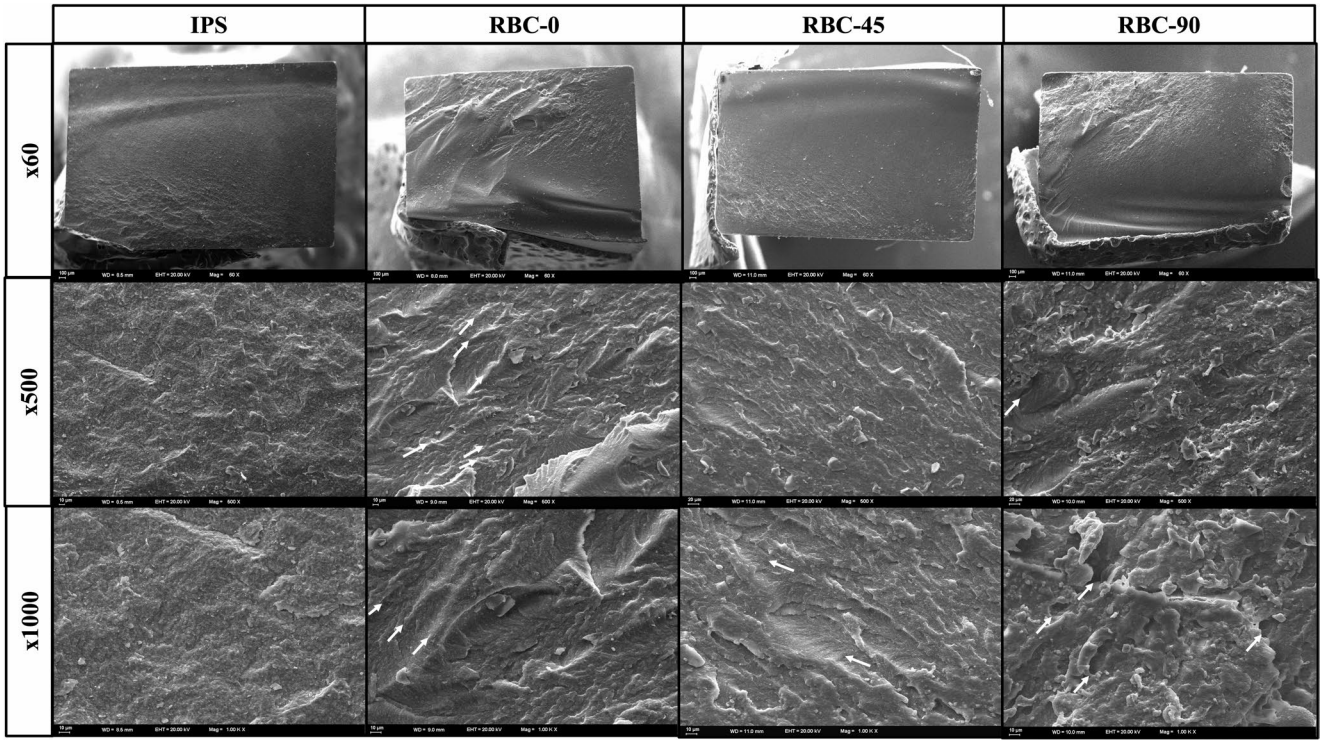


Fig. 3 Representative SEM micrographs displaying the fracture surface features of the test groups at magnifications of ×60, ×500, and ×1000. The IPS sample shows relatively homogeneous fracture surfaces. (RBC-0) Arrows indicate elongated grooves and a distinct lamellar (layered) structure. (RBC-45) Arrows point to intersecting crack paths and a directionless fracture pattern. (RBC-90) Arrows highlight surface micro-voids and fragmented regions

Regarding surface roughness, the IPS group (0.10 µm) presented the smoothest surface, whereas the 3D-printed RBC groups demonstrated higher roughness values ranging from 0.34 to 0.39 µm. However, build orientation did not produce a statistically significant effect on surface roughness within the 3D-printed RBC groups ($p > 0.05$).

Representative SEM images reflecting the surface characteristics of the test groups are presented in Fig. 2. Parallel scratch marks extending along the surface were observed in all groups and were more pronounced in the 3D-printed RBC groups. The quantitative surface roughness findings were consistent with the SEM based topographic observations. Micrographs of the IPS specimens revealed a homogeneous and compact morphology with preserved microstructural integrity (Fig. 2A). In contrast, the 3D-printed RBC groups exhibited periodic layer related striations and microscopic surface defects inherent to the additive manufacturing process, regardless of build orientation (Fig. 2B-D).

Fractographic evaluation of the fractured samples revealed surface characteristics that varied according to material type and printing orientation (Fig. 3). At low magnification (×60), brittle fracture features were observed in all groups, with visible differences in surface topography. The IPS and RBC-45 groups exhibited relatively planar and homogeneous fracture surfaces, whereas the RBC-0 and RBC-90 groups showed rougher and more irregular

morphologies. At higher magnification (×500), the IPS samples displayed fine and shallow surface features with limited microcracks. In contrast, the RBC-0 and RBC−90 groups demonstrated more pronounced surface irregularities characterized by elongated grooves, cleavage like features, and locally oriented fracture patterns consistent with the printing direction. The RBC-45 group showed an intermediate fracture morphology, with less directional organization. At ×1000 magnification, microstructural differences became more apparent. The IPS group maintained a relatively homogeneous fracture texture with small scale irregularities. RBC-0 samples showed prominent lamellar features and microcracks aligned with structural layers. The RBC-90 group exhibited increased microvoids, fragmented regions, and localized crack branching. RBC-45 samples demonstrated a more complex fracture surface defined by intersecting crack paths and reduced layer alignment.

Discussion

In this study, the mechanical and surface characteristics of reinforced 3D-printed RBCs at different printing orientations were evaluated in comparison with the lithium disilicate ceramic reference material, IPS e.max CAD. Overall, the findings indicated that significant differences were mainly related to the material type, whereas no notable variation was observed among the 3D-printed RBC groups, particularly in terms of elastic modulus and surface roughness. Accordingly, the first null hypothesis, which proposed that printing orientation would not influence mechanical properties, was partially rejected due to the differences detected in flexural strength and microhardness. In contrast, the second null hypothesis, which stated that surface roughness would not be affected by printing orientation, was accepted.

IPS e.max CAD is a lithium disilicate glass ceramic commonly used in clinical dentistry for a wide range of indications, including single crowns, inlays, onlays, veneers, and three unit fixed dental prostheses supported by a distal second premolar [27, 28]. Owing to its established clinical use and well described material properties [29], IPS e.max CAD offers a practical reference for the evaluation of emerging restorative materials [30, 31]. Since VarseoSmile TriniQ has been introduced for definitive restorative indications, including multi unit prosthetic applications [9], a comparison with an established ceramic system allows the findings to be interpreted within a clinically relevant context. In this context, IPS e.max CAD served as a suitable comparison material for the mechanical and surface characterization of the reinforced RBC system VarseoSmile TriniQ.

In this study, the ISO 6872:2015 protocol, which is accepted as the reference standard for ceramic materials, was adopted to enable a direct comparison between conventional glass-ceramic (IPS) and next-generation hybrid resin materials (RBC). Although VST is polymer-based, its relatively high ceramic filler content has led to the frequent use of ceramic testing standards for similar hybrid materials in the literature [14, 31–33].

The flexural strength represents the ability of a material to resist bending forces and corresponds to the maximum stress sustained before fracture [34]. The IPS group clearly exceeded the minimum flexural strength requirement of 100 MPa defined for ceramics in ISO 6872, whereas the VST groups showed values between 65 and 85 MPa. Therefore, the higher strength observed for IPS is consistent with expectations [31]. Lithium disilicate ceramics consist of approximately 70% fine lithium disilicate crystals dispersed within a glassy matrix [31]. This microstructure allows lithium disilicate to carry higher stresses within the same geometry due to its greater rigidity [28, 32]. In contrast, VarseoSmile TriniQ exhibit a hybrid structure composed of an organic matrix containing roughly 20–45 wt% silanized ceramic fillers [9]. In these materials, load transfer depends not only on matrix strength but also on interlayer bonding continuity, degree of photopolymerization, and the presence of micro-porosity or interfacial defects [31]. These structural differences explain why ceramic material demonstrate higher strength and stiffness, whereas 3D-printed RBC systems remain within a lower yet functionally relevant mechanical range. Even at its most favorable orientation (~ 85 MPa), the evaluated 3D-printed resin may therefore be more suitable for clinical applications with lower functional load demands rather than high load-bearing indications.

The printing orientation significantly influences the mechanical and physical behavior of additively manufactured materials due to their anisotropic nature [35]. In layered fabrication systems, material resistance is highly sensitive to the angle at which the critical tensile stress path intersects the interlayer boundaries, particularly at the lower surface, where the maximum tensile stress develops [36]. In the present study, the RBC group printed at 0° exhibited the highest flexural strength (85.96 MPa). This finding reflects the intrinsic anisotropic behavior of additively manufactured systems [35]. At 0° orientation, the printed layers were aligned parallel to the tensile stress generated during testing. Such alignment promotes crack propagation through the bulk of the material rather than along weaker interlayer interfaces, thereby enhancing mechanical resistance. In contrast, at 45° and 90° orientations, the layer arrangement relative to the loading direction may facilitate crack progression across multiple interlayer boundaries [31]. This configuration can increase susceptibility to early failure, even when the resin chemistry remains unchanged.

Recent evidence also indicates that build orientation plays a relevant role in the mechanical behavior of 3D-printed RBCs [13, 31]. In a study evaluating VarseoSmile TriniQ, Casucci et al. demonstrated that printing angulation significantly influenced flexural strength [13]. In contrast to the present findings, their results showed superior strength values at 45° rather than at 0°, highlighting that orientation-related performance may vary depending on specific experimental conditions and processing parameters. These differences are likely attributable to variations in printing conditions, specimen dimensions, and post-curing procedures, which directly affect layer cohesion and microstructural development. Since anisotropic behavior in 3D-printed RBCs is highly sensitive to processing variables, methodological differences between studies can reasonably lead to orientation-specific variations in mechanical performance.

The high value of the elastic modulus observed for IPS (approximately 77 GPa), reflects its pronounced rigidity and structural stability. The lower modulus values recorded for the VST groups indicate greater flexibility under masticatory loading. When appropriate post-curing and surface finishing procedures are applied, this controlled flexibility may offer a potential shock-absorbing effect, particularly in implant-supported restorations where occlusal loads are directly transferred to bone-supported structures. This behavior may contribute to a protective effect on opposing dentition; however, materials with reduced stiffness should be carefully selected in long-span restorations where higher rigidity is required. The findings of the present study indicate that the lack of significant differences in elastic modulus among the RBC groups, irrespective of printing orientation, suggests that stiffness is primarily governed by the polymer-ceramic filler ratio and the degree of polymerization rather than by the build orientation. Orientation-related effects appear to be more relevant to defect distribution and crack initiation behavior than to initial rigidity. Clinically, this indicates that the flexural response of VST under functional loading is expected to remain largely consistent regardless of the printing orientation.

Surface hardness is an important parameter when comparing restorative materials, as it reflects resistance to surface indentation and external wear. Hardness is primarily determined by the organic and inorganic composition of the material [31]. Because it is closely associated with wear resistance, it represents a critical requirement, particularly in posterior load-bearing regions [33]. In the present study, IPS exhibited the highest microhardness value, measuring 259.61 VHN. Within the RBC groups, the 90° printing orientation showed the highest surface hardness at 32.83 VHN. Considering the organic matrix structure of 3D-printed RBCs, differences in hardness are likely related to variations in filler content and filler–matrix interactions [31]. The marked difference between IPS and RBC can be explained by the relatively lower inorganic filler fraction of 3D-printed resins, which has previously been associated with softer and less rigid materials [31, 34]. Since hardness is closely linked to wear behavior, materials with higher hardness generally demonstrate greater resistance to surface degradation [37].

3D-printed RBCs exhibit anisotropic behavior, implying that their mechanical response varies according to the loading direction [35]. Previous evidence suggests that 0° and 90° build orientations can provide more favorable mechanical outcomes, whereas 45° may be less advantageous [38]. In the present study, the microhardness values followed the order RBC-90, RBC-0, and RBC-45. The relatively higher hardness observed at 90° may be related to layer alignment and polymerization efficiency at the tested surface, whereas the lower values at 45° could reflect altered interlayer organization. Variations in light exposure during layer-by-layer polymerization may contribute to this orientation-dependent performance [39]. These findings indicate that orientation-related anisotropy may also influence surface hardness, although the specific ranking may vary depending on the printing and post-curing conditions.

A rough surface promotes biofilm accumulation and increases susceptibility to bacterial colonization and periodontal inflammation [40]. According to Bollen et al. [41], a surface roughness of 0.2 µm represents the critical threshold for in-vivo bacterial retention, whereas the human tongue can perceive roughness values between 0.25 and 0.5 µm [42]. In the present study, IPS exhibited the lowest surface roughness value (0.10 µm), whereas the 3D-printed RBC groups showed higher values ranging from 0.34 to 0.39 µm, which is above the commonly reported 0.2 µm threshold. Because surface preparation in this study was limited to standardized grinding, these findings primarily reflect the baseline surface characteristics of the materials. From a clinical perspective, the higher roughness observed in the additively manufactured groups suggests that additional surface refinement procedures may be required before definitive clinical use.

Rojas-Rueda et al. evaluated the effect of surface treatments on 3D-printed crown materials and reported that polishing or varnish application reduced the Ra values to below 0.2 µm, with stability maintained after simulated toothbrushing [3]. This finding underscores the importance of finishing and polishing protocols in controlling surface roughness in additively manufactured restorations. Similarly, Tzimas et al. compared subtractively and additively manufactured restorative materials and noted that additively produced systems may present higher initial roughness due to their layered structure and limited surface finishing [1]. In both studies, VarseoSmile TriniQ was included among the evaluated materials, allowing for interpretation within a

comparable material context. However, in the present study, surface preparation was limited to standardized grinding, and no additional polishing or coating procedures were performed. This should be considered a limitation when interpreting the relatively higher Ra values observed in the 3D-printed RBC groups. In this context, further research is needed to clarify how clinically applied finishing and polishing procedures may influence the long-term surface behavior and overall performance of 3D-printed RBCs [43].

Recent studies have also indicated that the printing orientation may influence the surface roughness of 3D-printed resins [35, 44]. Shim et al. reported higher roughness values at a 45° orientation due to step-like layer formation, whereas other investigations observed lower roughness at 90° [44]. However, the present study did not reveal any difference in surface roughness values among the RBC groups. This discrepancy may also be related to differences in specimen design, surface preparation, and measurement methodology. These variables could have attenuated potential orientation-related surface irregularities in the present study.

The SEM micrographs obtained in this study demonstrated a clear correspondence between the microstructural features of the tested restorative materials and the quantitative surface roughness findings. The IPS group exhibited a homogeneous and compact surface morphology consistent with its dense crystalline microstructure, reflecting the regular surface characteristics of lithium disilicate ceramics. In contrast, the RBC groups displayed a layered architecture characteristic of additively manufactured materials, with periodic striations and localized microscopic surface defects, irrespective of the build orientation. The presence of a layer-by-layer structure and occasional spherical voids, previously described as typical features of 3D-printed resins, may account for the surface heterogeneity observed in the present study. Following standardized grinding, more pronounced parallel scratch patterns were evident in the RBC specimens. These features may be related to the material's wear resistance and lower surface hardness, as well as to the differential response of interlayer regions to mechanical finishing procedures in 3D-printed RBCs.

Fractographic evaluation confirmed the relationship between fracture behavior and build geometry at the microstructural level. The IPS specimens exhibited a relatively homogeneous and isotropic fracture pattern, consistent with the continuous crystalline network of lithium disilicate and its typical brittle failure mode. In contrast, the RBC groups showed greater morphological variability, reflecting the anisotropic nature of additively manufactured 3D-printed RBCs. The rough and irregular fracture surfaces observed in the RBC-0 and RBC-90 groups indicate that crack propagation was influenced by layer boundaries. In the 0° orientation, distinct lamellar features and layer-aligned microcracks suggest that crack growth occurred preferentially along the layer planes. In the 90° group, the presence of microvoids and localized crack branching points to tensile stresses acting across interlayer bonding regions during loading. The RBC-45 specimens demonstrated more randomly distributed microfeatures and intersecting crack paths. This pattern suggests that the 45° orientation may have deflected crack propagation and promoted a more complex energy dissipation mechanism. At higher magnification, these characteristic fracture features became more evident. Overall, the observed patterns support the influence of build orientation on interlayer cohesion and crack propagation resistance, and provide microstructural support for the mechanical findings of the present study.

This in-vitro study has several limitations. To standardize the experimental design, all specimens were produced with a uniform layer thickness of 50 µm and subjected to the same post-curing protocol. However, previous reports have shown that variations in layer thickness may influence flexural strength [31, 45]. Because layer thickness is directly related to the degree of conversion, it may affect not only mechanical performance but also long-term stability and biocompatibility [5]. An insufficient degree of conversion during post-processing can result in a weaker polymer network and reduced mechanical properties [46]. Furthermore, while the build orientations evaluated in this study 0°, 45° and 90°) represent the most widely accepted and clinically relevant standards in current dental literature to assess anisotropy [13, 47], testing only these distinct angles restricts the comprehensive screening of material behavior. Recent methodological advancements suggest that identifying mathematically calculated maximum allowable angles and screening a broader range of intermediate orientations could reveal critical performance boundaries [48]. In addition, as emphasized by Hoffmann et al., the performance of newly introduced restorative systems such as VarseoSmile TriniQ is not governed solely by material composition. It is also influenced by the specific interaction between the printer system and the resin formulation. The compatibility between light source characteristics, irradiation intensity, and resin chemistry plays a critical role in determining the final mechanical behavior [5]. Future investigations should therefore evaluate not only a wider spectrum of mathematical build angles, but also different printing technologies such as DLP, SLA, and LCD systems, together with their interactions with various resin formulations. Although thermal aging was applied, in-vitro conditions cannot fully reproduce the biological and functional complexity of the oral environment. To more accurately characterize the fracture behavior of 3D-printed RBCs compared with conventional systems, future studies should incorporate dynamic, fatigue-based protocols that better simulate multidirectional

and cyclic loading during clinical crown function. Accordingly, clinical validation through randomized controlled trials remains essential.

Conclusion

Within the limitations of this study, significant differences were observed in both the mechanical and surface properties.

- IPS e.max CAD demonstrated superior mechanical performance and lower surface roughness than the 3D-printed RBC.
- Build orientation did not significantly affect elastic modulus or surface roughness, whereas differences were observed in flexural strength and surface hardness.
- While the ceramic reference material (IPS) exhibited the highest overall mechanical strength and hardness, printing orientation was found to directly influence the flexural strength and microhardness within the 3D-printed groups. Specifically, the 0° printing orientation yielded the highest flexural strength, identifying it as the most durable orientation, whereas the 90° printing orientation achieved the highest microhardness values among the 3D-printed specimens.
- SEM analysis confirmed that the IPS group maintained a homogeneous and compact structure; in contrast, the 3D-printed groups exhibited a layered architecture and microscopic surface defects inherent to the additive manufacturing process, regardless of the build orientation. Furthermore, while the IPS group displayed a typical brittle fracture pattern, the 3D-printed RBC groups showed orientation-dependent and more complex fracture morphologies.

Clinical implication

While conventional ceramics such as IPS remain the gold standard for mechanical performance, 3D-printed RBCs offer a viable alternative when the build orientation is optimized. However, clinicians should be mindful that the layered architecture and microscopic defects inherent to 3D printing can result in orientation-dependent mechanical behavior under functional loading, unlike the more uniform and predictable structure of conventional materials.

Acknowledgements We gratefully acknowledge the financial support provided by Ankara University Scientific Research Projects Coordination Unit. The authors would also like to thank Mr. Mustafa Yeşil for his valuable technical assistance during the laboratory procedures.

Author contributions NEO (First author): conceptualization, methodology, validation, investigation, resources, data analysis, writing of the manuscript, and visualization. ZS: conceptualization, methodology, validation, investigation, resources, writing of the manuscript. MAK: conceptualization, methodology, writing of the manuscript, and visualization.

Funding Open access funding provided by the Scientific and Technological Research Council of Türkiye (TÜBİTAK). This study was supported by Ankara University Scientific Research Projects Coordination Unit (Project ID: 3575; Project Code: TSA-2024-3575).

Data availability The data that support the findings of this study are available from the corresponding author upon reasonable request.

Declarations

Conflict of interest The authors declare no conflicts of interest for the authorship and/or publication of this article.

Ethical approval This article does not contain any studies with human participants or animals performed by any of the authors.

Open Access This article is licensed under a Creative Commons Attribution 4.0 International License, which permits use, sharing, adaptation, distribution and reproduction in any medium or format, as long as you give appropriate credit to the original author(s) and the source, provide a link to the Creative Commons licence, and indicate if changes were made. The images or other third party material in this article are included in the article's Creative Commons licence, unless indicated otherwise in a credit line to the material. If material is not included in the article's Creative Commons licence and your intended use is not permitted by statutory regulation or exceeds the permitted use, you will need to obtain permission directly from the copyright holder. To view a copy of this licence, visit http://creativecommons.org/licenses/by/4.0/.

References

1. Tzimas K, Dimitriadi M, Rahiotis C, Pappa E. Surface characteristics of subtractively and additively manufactured restorative materials for definitive restorations. Mater (Basel). 2025;18:18.
2. Duarte S Jr., Phark JH. Advances in dental restorations: A comprehensive review of machinable and 3D-printed ceramic-reinforced composites. J Esthet Restor Dent. 2025;37(1):257–76.
3. Rojas-Rueda S, Alsahafi TA, Hammamy M, Surathu N, Surathu N, Lawson NC, et al. Roughness and gloss of 3D-printed crowns following polishing or varnish application. Materials. 2025;18(14):3308.
4. Quan H, Zhang T, Xu H, Luo S, Nie J, Zhu X. Photo-curing 3D printing technique and its challenges. Bioact Mater. 2020;5(1):110–5.
5. Hoffmann M, Coldea A, Stawarczyk B. Mechanical properties of novel 3D-printed restorative materials for definitive dental applications. Materials. 2025;18(20):4662.
6. Zattera ACA, Morganti FA, de Souza Balbinot G, Della Bona A, Collares FM. The influence of filler load in 3D printing resin-based composites. Dent Mater. 2024;40(7):1041–6.
7. Gekle S, Mayinger F, Kreitmair U, Reymus M, Hoffmann M, Stawarczyk B. Impact of different post-polymerization protocols on the material properties of three printed dental resins. J Mech Behav Biomed Mater. 2025;172:107164.
8. Arslan Acicbe B, Deniz S, Diken Türksayar AA, Dönmez MB, Demirel M. Fabrication and fit accuracy of definitive resin fixed

partial dentures additively manufactured using different vat polymerization technologies. J Dent. 2025;162:106052.
9. Bego GmbH. VarseoSmile TriniQ brochure. 2025. https://www.bego.com/fileadmin/user_downloads/Mediathek/3D-Druck/Materialien/VarseoSmile-TriniQ/EN/de_81036_0000_br_en.pdf. Accessed 16 Jul 2025.
10. Daghrery A, Vinothkumar TS, Majrashi H, Faqihi G, Gofshi R, Almasoudi S, et al. Dimensional accuracy of additive and subtractive manufactured ceramic-reinforced hybrid composite inlays: a CBCT-based in vitro study. Sci Rep. 2025;15(1):6048.
11. Dönmez MB, Demirel M, Diken Türksayar AA, Yilmaz B. Influence of printing parameters on the fabrication and fit accuracy of additively manufactured resin-based definitive three-unit fixed partial dentures. J Dent. 2025;161:105937.
12. VarseoWax® Model. https://www.bego.com/3d-printing/materials/varseowax-model/. Accessed 19 Jan 2026.
13. Casucci A, Verniani G, Sami Haichal W, Manfredini D, Ferrari M, Ferrari Cagidiaco E. Influence of printing angulation on the flexural strength of 3D printed resins: An in vitro study. Appl Sci. 2024;14(21):10067.
14. Sahin Z, Ozer NE, Yıkıcı C, Kılıçarslan MA. Mechanical characteristics of composite resins produced by additive and subtractive manufacturing. Eur J Prosthodont Restor Dent. 2023;31(3):278–85.
15. Chaiamornsup P, Iwasaki N, Tsuchida Y, Takahashi H. Effects of build orientation on adaptation of casting patterns for three-unit partial fixed dental prostheses fabricated by using digital light projection. J Prosthet Dent. 2022;128(5):1047–54.
16. Favero CS, English JD, Cozad BE, Wirthlin JO, Short MM, Kasper FK. Effect of print layer height and printer type on the accuracy of 3-dimensional printed orthodontic models. Am J Orthod Dentofac Orthop. 2017;152(4):557–65.
17. Jang G, Kim SK, Heo SJ, Koak JY. Fit analysis of stereolithography-manufactured three-unit resin prosthesis with different 3D-printing build orientations and layer thicknesses. J Prosthet Dent. 2024;131(2):301–12.
18. Unkovskiy A, Bui PH, Schille C, Geis-Gerstorfer J, Huettig F, Spintzyk S. Objects build orientation, positioning, and curing influence dimensional accuracy and flexural properties of stereolithographically printed resin. Dent Mater. 2018;34(12):e324–33.
19. Alghauli MA, Almutairi S, Almuzaini S, Aljohani R, Aljohani W, Alqutaibi AY. Properties and behavior of additively manufactured provisional fixed dental prostheses: A systematic review on 3D printing orientations relative to applied materials and postprocessing. J Esthetic Restor Dentistry. 2025;37(6):1407–18.
20. Gad MM, Fouda SM. Factors affecting flexural strength of 3D-printed resins: A systematic review. J Prosthodont. 2023;32(S1):96–110.
21. Hobbi P, Ordueri TM, Öztürk-Bozkurt F, Toz-Akalın T, Ateş M, Özcan M. 3D-printed resin composite posterior fixed dental prosthesis: a prospective clinical trial up to 1 year. Front Dent Med. 2024;5:1390600.
22. Caussin E, Moussally C, Le Goff S, Fasham T, Troizier-Cheyne M, Tapie L et al. Vat photopolymerization 3D printing in dentistry: A comprehensive review of actual popular technologies. Mater (Basel). 2024;17(4).
23. Turker Kader I, Ozer S, Arican B. Advanced 3D insights into the marginal and internal fit of ceramic-filled hybrid endocrowns with variable preparations. J Esthet Restor Dent. 2025;37(7):1753–61.
24. Turker Kader I, Ozer S, Arican B. An in vitro analysis of marginal and internal fit of 3D-printed permanent molar endocrowns with different preparation designs. Clin Oral Investig. 2025;29(6):319.
25. International Organization for Standardization. ISO 6872:2015 Dentistry - Ceramic materials. In: ISO Standards. International Organization for Standardization. 2015. https://www.iso.org/standard/59936.html
26. Zandinejad A, Das O, Barmak AB, Kuttolamadom M, Revilla-León M. The flexural strength and flexural modulus of stereolithography additively manufactured zirconia with different porosities. J Prosthodont. 2022;31(5):434–40.
27. Ivoclar. IPS e.max CAD. In: Ivoclar Products. https://www.ivoclar.com/tr_tr/products/digital-processes/ips-e.max-cad. Accessed 10 Mar 2026.
28. Oguz E, Kılıçarslan MA, Özcan M. Effect of endodontic access simulation on the fracture strength of lithium-disilicate and resin-matrix ceramic CAD-CAM crowns. J Esthet Restor Dent. 2020;32(5):472–9.
29. Oguz EI, Ozer NE. Recent advancements in glass ceramic materials. Turkiye Klinikleri Prosthodontics-Special Top. 2025;11(2):28–34.
30. Bataweel OO, Roulet JF, Rocha MG, Zoidis P, Pereira P, Delgado AJ. Effect of Simulated Tooth Brushing on Surface Roughness, Gloss, and Color Stability of Milled and Printed Permanent Restorative Materials. J Esthet Restor Dent. 2025;37(7):1773–83.
31. Lalvay EJA, de Carvalho FG, da Silva AR, Morganti FAC, Collares FM, Münchow EA. 3D-printed resins intended for long-term restoration vs. conventionally used materials: A systematic review and network meta-analysis of in vitro studies. J Dent. 2026;167:106531.
32. Özer NE, Şahin Z, Yıkıcı Çöl C, Arık Ö, Kılıçarslan MA. The effect of different staining solutions on the color stability of permanent indirect composite resins produced by additive and subtractive techniques. Meandros Med Dent J. 2024;25(3):262–78.
33. Temizci T, Bozoğulları HN. Effect of thermocycling on the mechanical properties of permanent composite-based CAD-CAM restorative materials produced by additive and subtractive manufacturing techniques. BMC Oral Health. 2024;24(1):334.
34. Bora PV, Sayed Ahmed A, Alford A, Pitttman K, Thomas V, Lawson NC. Characterization of materials used for 3D printing dental crowns and hybrid prostheses. J Esthet Restor Dent. 2024;36(1):220–30.
35. de Gois Moreira FG, Bezerra M, de Miranda LM, da Silva SEG, de Andrade Dantas EL, de Sousa FB, et al. Influence of build angle, printing layer thickness and aging on the flexural strength, precision, roughness and porosity analysis of a printed resin for provisional restorations. Odontology. 2025;113(3):1165–79.
36. Es-Said O, Foyos J, Mendelson M, Marloth R, Pregger BA. Effect of layer orientation on mechanical properties of rapid prototyped samples. Mater Manuf Processes. 2000;15:107–22.
37. Schönhoff LM, Mayinger F, Eichberger M, Reznikova E, Stawarczyk B. 3D printing of dental restorations: Mechanical properties of thermoplastic polymer materials. J Mech Behav Biomed Mater. 2021;119:104544.
38. Lins LBC, Leão RS, Pellizzer EP, Vasconcelos BCE, de Moraes SLD. Effect of three-dimensional print angle on integrity of interim crowns: A systematic review. J Prosthet Dent. 2025;134(5):1567–76.
39. Tahayeri A, Morgan M, Fugolin AP, Bompolaki D, Athirasala A, Pfeifer CS, et al. 3D printed versus conventionally cured provisional crown and bridge dental materials. Dent Mater. 2018;34(2):192–200.
40. Col CY, Sahin Z, Ozer NE, Kılıcarslan MA. The surface characteristics and micro-shear bond strength of resin cement to digitally produced permanent indirect resin composites: An in vitro study. Niger J Clin Pract. 2025;28(10):1213–24.
41. Bollen CM, Lambrechts P, Quirynen M. Comparison of surface roughness of oral hard materials to the threshold surface roughness for bacterial plaque retention: a review of the literature. Dent Mater. 1997;13(4):258–69.
42. Koizumi H, Saiki O, Nogawa H, Hiraba H, Okazaki T, Matsumura H. Surface roughness and gloss of current CAD/CAM resin

composites before and after toothbrush abrasion. Dent Mater J. 2015;34(6):881–7.
43. Kamonkhantikul K, Arksornnukit M, Lauvahutanon S, Takahashi H. Toothbrushing alters the surface roughness and gloss of composite resin CAD/CAM blocks. Dent Mater J. 2016;35(2):225–32.
44. Shim JS, Kim JE, Jeong SH, Choi YJ, Ryu JJ. Printing accuracy, mechanical properties, surface characteristics, and microbial adhesion of 3D-printed resins with various printing orientations. J Prosthet Dent. 2020;124(4):468–75.
45. Dizon JRC, Espera AH, Chen Q, Advincula RC. Mechanical characterization of 3D-printed polymers. Additive Manuf. 2018;20:44–67.
46. Schneider LF, Pfeifer CS, Consani S, Prahl SA, Ferracane JL. Influence of photoinitiator type on the rate of polymerization, degree of conversion, hardness and yellowing of dental resin composites. Dent Mater. 2008;24(9):1169–77.
47. Derban P, Negrea R, Rominu M, Marsavina L. Influence of the Printing Angle and Load Direction on Flexure Strength in 3D Printed Materials for Provisional Dental Restorations. Mater (Basel Switzerland). 2021;14(12):3376.
48. Zhao W, Singh P, Han J, Shen F, Hu K, Tsoi JKH. Precision-optimized process control in DLP printing of ultra-thin zirconia prostheses: A multi-factor accuracy analysis. Dent materials: official publication Acad Dent Mater. 2025;41(12):1609–19.

Publisher's Note Springer Nature remains neutral with regard to jurisdictional claims in published maps and institutional affiliations.